Article:
Kwon, MJ, Boyanov, MI, Yang, J-S et al. (2017) Transformation of zinc-concentrate in surface and subsurface environments: Implications for assessing zinc mobility/toxicity and choosing an optimal remediation strategy. Environmental Pollution, 226. pp. 346-355. ISSN: 0269-7491

https://doi.org/10.1016/j.envpol.2017.01.066

Transformation of zinc-concentrate in surface and subsurface environments: Implications for assessing zinc mobility/toxicity and choosing an optimal remediation strategy

Man Jae Kwon[a,b*], Maxim I. Boyanov[c,d], Jung-Seok Yang[a], Seunghak Lee[b,e], Yun Ho Hwang[a], Ju Yeon Lee[a,b], Bhoopesh Mishra[c,f], Kenneth M. Kemner[c]

[a] Korea Institute of Science and Technology, Gangneung, South Korea

[b] Green School, Korea University, Seoul, South Korea

[c] Biosciences Division, Argonne National Laboratory, Argonne, IL, USA

[d] Bulgarian Academy of Sciences, Institute of Chemical Engineering, Sofia, Bulgaria

[e] Korea Institute of Science and Technology, Seoul, South Korea

[f] Department of Physics, Illinois Institute of Technology, Chicago, IL, USA

*Corresponding Author: Korea Institute of Science and Technology, 679 Saimdangro, Gangneung, Gangwon-do, 210-340, Korea, Phone: +82-33-650-3705; Fax: +82-33-650-3729; mkwon@kist.re.kr

A manuscript submitted to Environmental Pollution

November 2016

Abstract

Zinc contamination in near- and sub-surface environments is a serious threat to many ecosystems and to public health. Sufficient understanding of Zn speciation and transport mechanisms is therefore critical to evaluating its risk to the environment and to developing remediation strategies. The geochemical and mineralogical characteristics of contaminated soils in the vicinity of a Zn ore transportation route were thoroughly investigated using a variety of analytical techniques (sequential extraction, XRF, XRD, SEM, and XAFS). Imported Zn-concentrate (ZnS) was deposited in a receiving facility and dispersed over time to the surrounding roadside areas and rice-paddy soils. Subsequent physical and chemical weathering resulted in dispersal into the subsurface. The species identified in the contaminated areas included Zn-sulfide, Zn-carbonate, other O-coordinated Zn-minerals, and Zn species bound to Fe/Mn oxides, as confirmed by XAFS spectroscopy and sequential extraction. The observed transformation from S-coordinated Zn to O-coordinated Zn suggests that this contaminant can change into more labile and dangerous forms as a result of weathering. For the purpose of developing a soil washing remediation process, the contaminated samples were extracted with dilute acids. The extraction efficiency increased with the increase of O-coordinated Zn relative to S-coordinated Zn in the sediment. This study demonstrates that improved understanding of Zn speciation in contaminated soils is essential for well-informed decision making regarding metal mobility and toxicity, as well as for choosing an appropriate remediation strategy using soil washing.

Capsule: More detailed information on the speciation and mineralogy of Zn at a particular location can enable a better assessment of metal mobility/toxicity and the choice of an optimal remediation strategy using soil washing.

Key words: Sphalerite; Heavy metal contamination; Acid extraction; Mineral transformation; XAFS

1. Introduction

Zinc (Zn), the fourth most common industrial metal, has been widely used in various applications such as galvanizing, alloys, brass and bronze materials. The worldwide production of Zn has increased to ca. 13 million tons per year in 2015 {USGS, 2015 #19}. The most significant Zn ores include sphalerite (ZnS) and smithsonite ($ZnCO_3$). Zinc sulfide is the most common Zn-concentrate {USEPA, 1997 #17} and is produced mainly by concentrating sphalerite (ZnS) using froth flotation techniques. Although Zn is one of the essential elements for living cells, an excess amount of Zn can pose serious toxicity to human health as well as to the ecosystem {Fosmire, 1990 #20;Jacquat, 2009 #46}. The regulatory limits (termed the precaution level and the action level) of Zn in soil of South Korea are 300 and 900 mg/kg, respectively {Environment, 2009 #52}. However, the toxicity of heavy metals depends not only on the total concentration, but also on the speciation of the metal {Jacquat, 2009 #46}. For example, labile Zn species (i.e., weakly bound to soil surfaces) are known to be more toxic than strongly bound Zn species because the labile species transport easily through the soil and sediment and are also readily bioavailable for plants and microorganisms {Alloway, 1995 #47}. In addition, a recent study {Kwon, 2015 #49} investigated microbial community compositions in the sediments with extremely high and relatively low concentrations of heavy metals near mine tailing sites and showed that microbial community structure was strongly affected by more labile form of Pb and/or Zn, rather than by stable form of As in spite of extremely high concentrations of total As (~10%).

The speciation and mineralogy of Zn in surface and subsurface environments is determined by long-term physical and chemical weathering processes {Sonke, 2002 #16;Priadi, 2012 #23} which are in turn controlled by the specific conditions in the system {Jacquat, 2009 #46}. Therefore, the characterization of Zn speciation at geochemically diverse locations is an essential part of understanding the factors controlling its long-range mobility and there have been several studies focusing on the Zn transformations at particular field sites. For instance, a past study reported that the rapid diagenetic transformation of atmospheric Zn in anoxic subsurface environments resulted in the formation of Zn sulfides {Sonke, 2002 #16}. Zinc speciation has also been investigated in the context of its mobility during long-term weathering of mine tailings {Root, 2015 #45;Shim, 2015 #48;Kwon, 2015 #49}. In

addition, the study by Priadi et al. {Priadi, 2012 #23} investigated the sources and cycling processes of Zn in a river basin and showed that Zn speciation in suspended particulate matter (SPM) varied significantly between upstream and downstream sections of the river.

In places where Zn contamination has occurred in soil and sediments, various physical and chemical remediation techniques have been employed. Among them, ex-situ soil washing has been frequently used because many contaminants can be completely and rapidly removed below the regulatory limits {Wuana, 2011 #18}. However, in some cases, the heavy metals in contaminated soils and sediments are sparingly soluble and present in strongly bound forms (e.g., in sulfide or in extraction-resistant fractions){Wuana, 2011 #18}. A variety of chemical agents can be used to extract the contaminants from soils (e.g., strong acid, chelating agents, organic acids, surfactants). Strong acids have been widely and successfully used as they effectively release heavy metals and dissolve even crystalline forms of contaminants {Wuana, 2011 #18}. For a more targeted and efficient treatment, the site-specific data on metal speciation and mineralogy must be considered because this information can provide important insight on the type and concentrations of the eluent to be used. Although several studies have investigated the effectiveness of soil washing for treating Zn-contamination in terms of soil particle sizes and the specific washing agents {Dermont, 2008 #27;Gusiatin, 2012 #26;Race, 2016 #25}, little is known about how Zn speciation and mineralogy affect the remediation efficiency of sediments with extremely high concentrations of Zn during a soil washing process. To achieve efficient remediation at a particular site, the site-specific Zn speciation and mineralogy should be considered and understood before conducting risk assessments and remediation strategies due to the strong dependency of Zn mobility and bioavailability to Zn speciation and mineralogy {Roberts, 2002 #41}.

This study investigated the geochemical and mineralogical characteristics of Zn-contaminated soils around a Zn-ore transportation route to (1) understand the transformations and transport of Zn-concentrates in the near- and sub-surface region, (2) identify the major Zn species and mineral phases, and (3) determine the optimal remediation strategy for these sediments using a soil washing process with inorganic acids. Zn-contaminated soil samples, as well as Zn-concentrate samples near the roadside and surrounding environments were collected and the speciation of Zn was examined using a

variety of analytical techniques including sequential extraction, X-ray Fluorescence (XRF) spectroscopy, X-ray Diffraction (XRD), Scanning Electron Microscopy (SEM), and X-ray Absorption Fine Structure (XAFS) spectroscopy.

2. Material and methods

2.1. Study area and sampling method

The study site is located in the eastern part of South Korea (Fig. 1). Zinc-concentrates (ores that contain Zn) were imported and stored there from 1999 until 2016. The concentrates were transported to Zn smelters around the country to be converted into pure Zn. However, large amounts of Zn-concentrates (in the form of fly dust) were left behind during the daily transportation by dump trucks or trains. Therefore, extremely high levels of Zn are now present in the surrounding soils and sediments (approximately 25,600 m^3), which can be a long-term source of Zn release to the environment and ecosystems in the area.

In June 2015, one sample of Zn-concentrate, one sample of roadside dust, and eight samples from surrounding soils were collected with a stainless steel shovel. Soil samples were collected after removal of the overlying few centimeters of aerobic topsoil. In addition, unsaturated subsoil samples from the subsurface were collected at three depths of 0-15, 15-30, and 30-50 cm. The soil color was determined by comparisons with the Munsell soil color chart.

2.2. Chemicals

The acids used to prepare the soil washing solutions were 37% HCl and 70% HNO_3 purchased from Dongwoo Fine Chem Co. (S. Korea), as well as 98% H_2SO_4 and 85% H_3PO_4 purchased from Daejung Co. (S. Korea). All other chemicals used were of reagent grade quality or higher. Distilled deionized water (ddH_2O)(> 18.2 MΩ·cm) from a Millipore ultrapure water purification system (Barnstead, USA) was used throughout. All analytical procedures were validated by using certified and/or internal reference materials.

135 *2.3. Physical, chemical, and mineralogical analyses*

136 Loss on ignition was determined gravimetrically by heating the samples at 600 °C for 6 h in a
137 muffle furnace. To determine soil pH, a mixture of soil and deionized water (= 1:5 g) was shaken for
138 about 2-3 minutes and then allowed the soil to settle for 2 minutes. The pH of the soil suspension was
139 measured with a pH meter (Mettler Toledo, USA) using a glass electrode. For the analysis of elemental
140 distributions in dust and soil samples, the samples were air dried, sieved to 10 mesh (< 2 mm), quartered,
141 and pulverized to 80 mesh (< 180 μm). The concentrations of major and trace elements in bulk samples
142 were determined by wavelength-dispersive X-ray fluorescence (XRF) at the Korea Basic Science
143 Institute. The total concentrations of toxic metals in bulk samples were also determined by *aqua regia*
144 digestion (HNO_3 : HCl = 1 : 3 v/v). The conventional Tessier sequential extraction procedures {Tessier,
145 1979 #22} were also applied to determine Zn and Pb fractionation in the soil samples. The
146 concentrations of As, Zn, Pb, Cu, Ni, and Cd were determined by inductively coupled plasma optical
147 emission spectrometry (ICP-OES, Varian 730-ES, USA). The analytical conditions of these metals
148 using ICP-OES are summarized in Table S1.

149 Surface analysis of the samples was conducted with scanning electron microscopy (SEM)(S-
150 3000H, Hitachi, Japan) at Korea Institute of Science and Technology, S. Korea. SEM backscattered
151 electron images were collected at 3000 × magnification.

152 X-ray powder diffraction (pXRD) analysis was conducted to identify crystalline phases in bulk
153 samples from the mine tailings. The pXRD data were collected with an X'Pert Pro MPD X-ray
154 diffractometer with Ni-filtered Cu Kα radiation. The samples were scanned between 10° and 80° 2θ at
155 a speed of 2.5° 2θ min-1. The pXRD patterns were analyzed with the JADE 6 software package (MDI,
156 Livermore, CA, USA).

157 Zinc K-edge (9,659 eV) x-ray absorption near-edge (XANES) and extended x-ray absorption
158 fine-structure (EXAFS) spectra were collected at room temperature in transmission and fluorescence
159 mode at sectors 10-BM, MRCAT/ EnviroCAT beamline, Advanced Photon Source, Argonne National
160 Laboratory, Illinois, USA {Kropf, 2010 #10}. The incident energy was scanned by using the Si(111)
161 reflection of the double-crystal monochromator in step-scanning mode (approximately 15 min per scan

for the extended region). Soil samples were collected and kept sealed in plastic centrifuge tubes under ambient conditions. Eight samples were examined, two with significantly higher Zn concentration, and six samples of lower concentration. The higher concentration solids were mounted dry on the sticky side of Kapton tape. The lower concentration solids were size-fractioned using the following procedure. About 2 grams of the original material was suspended in 10 mL DI water in equilibrium with air, homogenized on a Vortex shaker for 30 s, and allowed to settle for 1 minute. The solution and suspended solids that remained at the top (termed "fine fraction") were separated from the suspension using a pipette. The fine fraction solids were filtered from the new suspension using a 0.22 μm nylon membrane. The hydrated filter cake and the membrane were placed between Kapton film for the x-ray measurements. Zinc remaining in the pore solution of the solids has an insignificant contribution to the measured spectra under our experimental conditions. X-ray absorption spectra from dissolved Zn salts and polycrystalline Zn oxides, hydroxides, phosphates, carbonates, and sulfides were collected as standards for the XANES and EXAFS analysis. All spectra were aligned on the energy axis using the reference spectrum (Zn metal foil) taken simultaneously with the sample and standards spectra. Normalization and background subtraction was done using the program AUTOBK {Newville, 1993 #12}. Data were Fourier transformed (FT) by using the FEFFIT program {Newville, 1995 #13}. Identical transform parameters were used for the standards and the unknown spectra (e.g., k-weighting, Fourier transformation range, and 1.0 $Å^{-1}$ Hanning window functions).

2.4. Extraction efficiency of zinc from contaminated soils using strong acids

Approximately 2.5 g of air-dried 10-mesh sieved (< 2 mm) dust and soil samples were added into 50-mL conical tubes containing 25 mL of washing acids (0.1 N or 1.0 N of HCl, HNO_3, H_2SO_4, and H_3PO_4) and incubated on a shaker at 120 rpm and 20°C for 1 hour. All tests were performed in duplicate. The suspensions were filtered through a 0.45 μm filter membrane and the supernatants were analyzed by ICP-OES.

188 **3. Results and discussion**

189 *3.1. Geochemical characteristics*

190 The determined chemical composition of the samples are shown in Table 1. Except for the Zn-
191 concentrate and the road dust samples, the elemental concentrations are in the following order: O > Si
192 > Al > Fe > K ≈ Mg ≈ Ca. In all samples except the samples collected at 40-50 cm depths, Zn
193 concentrations exceeded the soil regulatory guidelines (i.e., the precaution level > 300 mg/kg, the action
194 level > 900 mg/kg) {Environment, 2009 #52}. Samples collected near the surface also showed Cd
195 contamination (the precaution level > 4 mg/kg, the action level > 12 mg/kg) {Environment, 2009 #52}.
196 Roadside dust and railroad side soil samples (MJK-2 and MJK-4) showed extremely high
197 concentrations of As, Cu, and/or Pb (the precaution levels and the action levels of these toxic metals
198 are > 25 and > 75 mg/kg for As, > 150 and > 450 mg/kg for Cu, > 200 and > 600 mg/kg for Pb,
199 respectively) {Environment, 2009 #52}. Two of the samples collected from otherwise similar sampling
200 environments at the surface near the railroad showed significantly different toxic metal concentrations
201 (samples MJK-3 and MJK-4, Fig. 1). It is likely that the lower metal concentrations in MJK-3 resulted
202 from the blocking of dust deposition at the site of sample MJK-3 by a long fence running parallel to the
203 railroad.
204 The soil pH was neutral to slightly alkaline (measured pH was between 7 and 8.7). Loss on
205 ignition (%) ranged between 0.6 and 7.7 %.
206

207 *3.2. Mineralogy*

208 *3.2.1. X-ray powder diffraction*

209 The XRD patterns indicated that the major crystalline phases of Zn-concentrate (MJK-1) was
210 sphalerite (Zn,Fe)S and those of roadside dust (MJK-2) were quartz (SiO_2) and Fe-rich sphalerite (Table.
211 1). This suggests that Zn contamination in the roadside dust is a simple mechanical mixture between
212 the native minerals and the Zn-concentrates, without any chemical weathering. Calcite was also

observed in the roadside dust samples likely because of the release of calcite-rich particles during the ground transportation of limestones by trucks and trains in this area.

3.2.2. X-ray absorption fine structure

Figure 2 compares the XANES and EXAFS data obtained from the Zn-concentrate, dust, and soil samples to Zn standards measured at the same beamline during a previous study {Dimkpa, 2013 #6}. A clear trend in the spectral features can be observed, with samples MJK-1 and MJK-6-2 representing the endmember spectra. The trend suggests that the predominant Zn speciation at the different sample locations is changing between two major species (described below).

Comparisons of endmember spectrum MJK-1 to standards show that Zn in this sample is present as S-coordinated Zn(II) species. Analogously to the spectral trends in Fe minerals {O'Day, 2004 #51}, the XANES spectra of S-coordinated Zn show a lower edge energy position and a suppressed white line intensity (the first peak after the edge), whereas the XANES of O-coordinated Zn generally show a higher edge energy position and a larger white line amplitude [19]. The features in the XANES spectrum of MJK-1 are nearly identical to those of the polycrystalline sphalerite standard, ZnS (Fig. 2); however, the amplitude of the white line (peak immediately after the absorption edge) is smaller. Despite the spectral features being nearly identical to those of the ZnS standard, amplitude suppression was also observed in the EXAFS data (Fig. S1). The x-ray absorption data from this sample were collected in transmission mode. Thus, the likely causes are thickness and pin-hole effects due to the presence of highly concentrated ZnS particles, much larger than multiple x-ray absorption lengths, mixed with the larger soil particles {Manceau, 2002 #28}. The images from the SEM analysis also indicate the presence of micron-sized entities in the presence of larger soil particles (Fig. S2).

The similarity of endmember spectrum MJK-6-2 to O-coordinated Zn standards shows that Zn in this sample is present as O-coordinated Zn(II) species (Fig. 3). The features in the XANES spectrum are also more similar to those of standards where Zn(II) is predominantly octahedrally coordinated to O, OH, or H_2O atoms, and in which the ligand does not bind strongly to the Zn(II) atom, such as in the Zn acetate aqueous solution standard or the hydroxy-salts of Zn (Zn-OH-Cl or hydrozincite Zn-OH-

CO_3). However, none of the available standards matches the MJK-6-2 spectrum to an extent where an exact identification of the Zn species can be established. The shape and phase of the features in the EXAFS data allow exclusion of $ZnCO_3$, ZnO, and $Zn_3(PO_4)_2$ in sample MJK-6-2, based on the lack of the strong features seen in the Fourier transform (FT) of these standards between 2 and 6 Å (Fig. 4) or based on the Zn-O distance (position of peak "a" in Fig. 4). ZnO has Zn(II) in tetrahedral coordination by O (R_{Zn-O}~1.98 Å), whereas the aqueous solution or the hydroxyl-salts have Zn in octahedral coordination by O (R_{Zn-O}~2.11 Å){Ghose, 1964 #7;Graf, 1961 #14;Kihara, 1985 #9}. Zinc(II) coordination in silicate minerals (e.g. willemite) is also tetrahedral {Marumo, 1971 #11}. Hence, a tetrahedral O coordination of Zn can be excluded in sample MJK-6-2 based on the Zn-O distance and the corresponding position of the FT peak (Fig 4). Tetrahedral Zn(II) phases such as Franklinite (Zn ferrite, $ZnFe_2O_4$, which can be thought of as Zn-substituted magnetite) can also be excluded. The EXAFS data therefore indicate that Zn(II) in the MJK-6-2 sample is present predominantly in octahedral geometry. Zinc coordination in Zn-sulfates (e.g. in Bianchite, Boyleite, or Goslarite) is octahedral {Anderson, 2012 #5} and has been observed in mine tailings with increased acidification {Hayes, 2011 #8}. Although the Zn-O distance in MJK-6-2 is similar to that in Zn-OH-Cl, Zn-OH-CO_3, or Zn-OH-SO_4, all of the latter standards show a signal between R+Δ=2.5-3.2 Å (feature "b" in Fig. 4), which corresponds to the bidentate Zn-Zn coordination in hydroxy-zincite (Zn-OH-CO_3). This signal is absent in the spectrum of MJK-6-2, suggesting lack of Zn-Zn coordination. Instead, spectrum MJK-6-2 has peaks between R+Δ=3.5-4.5 Å (feature "c" in Fig. 4), which are not seen in the above standards, as well as in the aqueous Zn-acetate standard. From these observations we conclude that octahedrally coordinated Zn(II) is present in a single phase that is disordered or that there are several octahedrally coordinated Zn(II) species present in the sample.

3.3. Fate and transport of zinc-concentrates

Zn-concentrate, mainly as [(Zn,Fe)S], transformed to Zn species of various lability as a result of physical and chemical weathering. Tessier sequential extraction of sample MJK-1 showed that it was mostly composed of Zn fractions F3 (12%), F4 (28%), and F5 (60%)(F1: exchangeable, F2: bound to

carbonates, F3: bound to iron and manganese oxides, F4: bound to organic matter, F5: residual). As a result of the weathering process, fraction F2 increased, but fraction F5 decreased in samples MJK-2 to MJK-6-3 (Fig. 5).

The solubility of Zn minerals in water depends strongly on crystallinity and particle size {Clever, 1992 #21}. In general, Zn-acetate, -nitrate, -sulfate, -chloride, -chlorate and -perchlorate are very soluble in water, while Zn-oxide, -carbonate and -sulfide are slightly soluble or insoluble in water. The solubility of Zn also depends on temperature and on the pH of the solution. At neutral pH, Zn minerals in water are less soluble, but the solubility increases with increasing acidity and above pH 11 {Permyakov, 2009 #53}. Given the neutral pH and the wide distribution of ZnS in the study area, the solubility of the Zn mineral phases is likely very low (The reported solubilities of ZnS based on model calculation or colorimetric analysis ranged between 3×10^{-10} and 1×10^{-7} mol L^{-1} at pH 7){Clever, 1992 #21}, but long-term weathering can cause the slow dissolution of these mineral phases and subsequent contamination of the subsurface environment.

In subsurface environments, aqueous Zn (i.e., $ZnOH^{+}_{(aq)}$ or $Zn^{2+}_{(aq)}$) can be retarded by sorption to various mineral or biological surfaces {Lee, 2014 #15}. The vertical distribution of metal concentrations clearly showed that the concentrations of toxic metals decreased with depth (Fig. 6). The concentrations of Zn at the depths of 0-30 cm was much higher than that of the soil regulatory guidelines of S. Korea. The concentrations of Zn in MJK-5 decreased from 1,689 mg kg^{-1} at the depth of 0-15 cm to 923 mg kg^{-1} at the depth of 15-30 cm, while those in MJK-6 decreased from 3,551 mg kg^{-1} at the depth of 0-15 cm to 722 mg kg^{-1} at the depth of 15-30 cm. At the depth of 30-50 cm, the concentrations of Zn in both locations were below the guideline. These results suggest that Zn species originating from the Zn-concentrate (MJK-1) are not transported vertically on the meters length scale over the 10 year time period between the deposition of the concentrate and the transformation to more mobile species in soil samples. However, this does not mean that groundwater quality around the study area is safe to the public, as this reservoir of Zn in the solids could be mobilized due to a seasonal or other change in geochemical conditions. More importantly, a very small concentration in groundwater can pose a substantial risk to both human and ecosystem health; a regulatory guideline of Zn is 3 mg L^{-1}

294 {Environment, 2009 #52}. Given that Zn-concentrate and labile O-coordinated Zn species are widely
295 distributed in the contaminated soil samples, toxic level of Zn could be present in groundwater. The
296 result of a leaching experiment also supports this since the extent of Zn released from Zn-concentrate
297 with artificial rainwater was 10 mg L^{-1} (Fig. S3).

298 Sequential extraction results indicated that the F3 fraction increased, whereas the F4 fraction
299 decreased with depth (Fig. 5). This suggests that Zn bound to sulfide transformed into Zn bound to Fe
300 and/or Mn oxides with depth. The subsequent increase in F4 and F5 Zn fractions at 30-50 cm depth are
301 likely not due to the influence of Zn from shallower depths, but likely due to the presence of F4 and F5
302 Zn fractions in the original soil itself. The concentrations of F4 and F5 in MJK-5-3 and MJK-6-3 were
303 only < 45 and < 75 mg kg^{-1}, respectively.

304 The transformation of Zn-concentrate during the weathering process is confirmed by the
305 XAFS analysis. The gradual spectral trends observed in Fig. 2 were interpreted by linear combination
306 (LC) analysis, using the spectra from MJK-1 and MJK-6-2 as endmembers. This analysis quantified the
307 proportion of total Zn in each of the endmember species (MJK-1 and MJK-6-2) in samples MJK-2 to
308 MJK-6-1. The LC fits are shown in Fig. S4. The best fit component fractions are summarized in Table
309 2 and are interpreted as "proportion of S- vs. O- coordinated Zn(II) species". It appears that the more
310 the soil samples undergo weathering processes from the source or migrate from the surface of the soil,
311 the more the immediate coordination of Zn(II) changes from S-bound to O-bound. As discussed earlier,
312 endmember MJK-1 represents S-coordinated Zn as in ZnS, whereas endmember MJK-8 represents O-
313 coordinated Zn.

314 In summary, dispersed Zn-concentrate (ZnS) was deposited on the surface and Zn ions
315 resulting from dissolution of the concentrate infiltrated in the underlying soil. The dissolved Zn(II)
316 either adsorbed on particle surfaces or were complexed by various anions available in the subsurface
317 environments (particularly, carbonates), which likely resulted in precipitation of the corresponding
318 mineral.

319

320 *3.4. Zinc extraction from contaminated soils by diluted inorganic acids*

321 Correlation plots between the XAFS, acid extraction, and sequential extraction results are
322 shown in Fig. 7. Sum of the F1 to F3 fraction of Pb is not correlated with the extent of Pb extracted by
323 acids (Fig. 7A). However, Zn concentrations determined by acid extraction showed high correlation
324 coefficients with those determined by sequential extraction (F1 to F3) (r^2 = 0.93 - 0.98) (Fig. 7B). This
325 suggests that when Zn is present more in F1 to F3 fraction of soil samples than in the F4-F5 fraction,
326 the extent of Zn extraction by acids is higher (Fig. 7B). Moreover, these results clearly indicate that Zn
327 in the soil samples originated from other sources (i.e., Zn-concentrate, ZnS) and transformed as F1 to
328 F3 forms. The spectral proportion of O-coordinated Zn from LCF (Linear Combination Fit) also showed
329 a linear correlation (r^2 = 0.96) with the sum of F1 to F3 Zn fraction (Fig. 7C). The spectral proportions
330 of O-coordinated Zn species is higher than the F1 to F3 Zn fraction (e.g., 59% of spectral proportions
331 of O-coordinated Zn species vs 25% of F1 to F3 Zn fraction) because LCF analysis accounted onlyS-
332 coordinated and O-coordinated Zn species. Obviously, other mineral phases other than those species
333 may be present in the soil samples. The comparison between acid extraction, sequential extraction, and
334 XAFS analysis provides important information that the extent of metal extraction from long-term
335 weathered soils can be estimated based on these different analytical methods.

336 The results also show that higher concentrations of acids can extract more Zn and Pb from the
337 contaminated soils (Fig. 7B and 7D); however, the extent of Zn and Pb extraction were dependent on
338 the specific types of acids. HCl was the most effective to extract Zn and Pb from the soil, while H_3PO_4
339 was the least effective. The efficiency of Zn extraction also clearly increased with the increase in F1 to
340 F3 fraction by sequential extraction or O-coordinated Zn speciation determined by XAFS analysis. Both
341 1.0 N HCl and 1.0 N H_2SO_4 extracted approximately 80% of Zn from the contaminated soils with 58%
342 F1 to F3 Zn fraction, while extracted only 48% of Zn from the contaminated soils with 45% F1 to F3
343 Zn fraction.

344 Most metal-oxides, -carbonates and -sulfides are insoluble or sparingly soluble in water, but
345 soluble in dilute acids. Therefore, soil washing by acid extraction has been widely applied to various
346 contaminated sites {Alghanmi, 2015 #2;Ko, 2006 #3}. However, there has been little or no study

investigating the combined effects of acid type, acid concentration, and metal speciation/fractions on the extent of metal leaching. The results in the current study imply that metal species and mineral phases play a critical role in extracting metals from contaminated soils. The results also provide basic information on the type of remediation approaches that can yield successful remediation outcomes, and show that the specific acids and their concentrations should be carefully selected based on the metal speciation/fractionation and mineral phases. In the specific soils particularly with high proportion of O-coordinated Zn species, 1.0 N (or higher) HCl would be the most effective acid for leaching Zn from the contaminated soils.

4. Conclusions

The shipping and processing of Zn-concentrates can cause the dispersal of Zn contamination in the surrounding surface and subsurface environments. Our study shows that Zn accumulated in soils can transform during long-term weathering and as a result may be distributed in Zn species and mineral phases of various stability. At our particular site, Zn-concentrate (ZnS) was deposited directly to the soil surface during vehicle transportation and later transformed to various mineral phases depending on the local geochemical conditions and the dominant primary mineral phases. Overall, the Zn species/minerals at our site underwent the transformation from Zn sulfides → O-coordinated Zn. The semi-quantitative analysis of Zn species and mineral phases using XAFS and sequential extraction allowed for establishing a correlation between dilute acid extractability and Zn speciation. Hydrochloric acid (1.0 N) was most effective among acids tested for leaching Zn from the contaminated soils with high proportion of O-coordinated Zn species. Our study demonstrates that more detailed information on the speciation and mineralogy of contaminant metals at a particular location can enable a better assessment of metal mobility/toxicity and the choice of an optimal remediation strategy using soil washing.

Acknowledgement

We thank Daehoon Lee and Joonwoo Park, Hayoung Yoo for help during the sample collection and analysis. Research under the Subsurface Biogeochemical Research Program Scientific Focus Area (SFA) at Argonne National Laboratory was supported by the Subsurface Biogeochemical Research Program, Office of Biological and Environmental Research (BER), Office of Science, U.S. Department of Energy (DOE), under contract DE-AC02-06CH11357. MRCAT/EnviroCAT operations are supported by DOE and the member institutions. Use of the Advanced Photon Source, an Office of Science User Facility operated for the U.S. Department of Energy (DOE) Office of Science by Argonne National Laboratory, was supported by the U.S. DOE under Contract No. DE-AC02-06CH11357. This work also was supported by and Korea Ministry of Environment as The GAIA Project-2015000540001, and a National Research Foundation of Korea Grant funded by the Korean Government (MSIP) (2016, University-Institute cooperation program).

384 **References**

385 [1] USGS, Mineral Commodity Summaries, in, 2015.
386 https://minerals.usgs.gov/minerals/pubs/mcs/2015/mcs2015.pdf, accessed on January 14, 2017
387 [2] USEPA, BACKGROUND REPORT AP-42 SECTION 12.7 PRIMARY ZINC SMELTING, in,
388 1997. https://www3.epa.gov/ttn/chief/ap42/ch12/bgdocs/b12s07.pdf, accessed on January 14,
389 2017
390 [3] G.J. Fosmire, Zinc toxicity, The American Journal of Clinical Nutrition, 51 (1990) 225-227.
391 [4] O. Jacquat, A. Voegelin, R. Kretzschmar, Soil properties controlling Zn speciation and fractionation
392 in contaminated soils, Geochimica et Cosmochimica Acta, 73 (2009) 5256-5272.
393 [5] B.J. Alloway, Heavy Metals in Soils, Blackie Academic & Professional, 1995.
394 [6] M.J. Kwon, J.-S. Yang, S. Lee, G. Lee, B. Ham, M.I. Boyanov, K.M. Kemner, E.J. O'Loughlin,
395 Geochemical characteristics and microbial community composition in toxic metal-rich sediments
396 contaminated with Au–Ag mine tailings, Journal of Hazardous Materials, 296 (2015) 147-157.
397 [7] J.E. Sonke, J.A. Hoogewerff, S.R. van der Laan, J. Vangronsveld, A chemical and mineralogical
398 reconstruction of Zn-smelter emissions in the Kempen region (Belgium), based on organic pool
399 sediment cores, The Science of the Total Environment, 292 (2002) 101-119.
400 [8] C. Priadi, P. Le Pape, G. Morin, S. Ayrault, F. Maillot, F. Juillot, R. Hochreutener, I. Llorens, D.
401 Testemale, O. Proux, G.E. Brown, X-ray Absorption Fine Structure Evidence for Amorphous Zinc
402 Sulfide as a Major Zinc Species in Suspended Matter from the Seine River Downstream of Paris,
403 Ile-de-France, France, Environmental Science & Technology, 46 (2012) 3712-3720.
404 [9] R.A. Root, S.M. Hayes, C.M. Hammond, R.M. Maier, J. Chorover, Toxic metal(loid) speciation
405 during weathering of iron sulfide mine tailings under semi-arid climate, Applied Geochemistry,
406 62 (2015) 131-149.
407 [10] M.J. Shim, B.Y. Choi, G. Lee, Y.H. Hwang, J.-S. Yang, E.J. O'Loughlin, M.J. Kwon, Water quality
408 changes in acid mine drainage streams in Gangneung, Korea, 10 years after treatment with
409 limestone, Journal of Geochemical Exploration, 159 (2015) 234-242.

[11] R.A. Wuana, F.E. Okieimen, Heavy Metals in Contaminated Soils: A Review of Sources, Chemistry, Risks and Best Available Strategies for Remediation, ISRN Ecology, 2011 (2011) 20.

[12] G. Dermont, M. Bergeron, G. Mercier, M. Richer-Laflèche, Soil washing for metal removal: A review of physical/chemical technologies and field applications, Journal of Hazardous Materials, 152 (2008) 1-31.

[13] Z.M. Gusiatin, E. Klimiuk, Metal (Cu, Cd and Zn) removal and stabilization during multiple soil washing by saponin, Chemosphere, 86 (2012) 383-391.

[14] M. Race, R. Marotta, M. Fabbricino, F. Pirozzi, R. Andreozzi, L. Cortese, P. Giudicianni, Copper and zinc removal from contaminated soils through soil washing process using ethylenediaminedisuccinic acid as a chelating agent: A modeling investigation, Journal of Environmental Chemical Engineering, 4 (2016) 2878-2891.

[15] A. Tessier, P.G.C. Campbell, M. Bisson, Sequential extraction procedure for the speciation of particulate trace metals, Analytical Chemistry, 51 (1979) 844-851.

[16] A.J. Kropf, J. Katsoudas, S. Chattopadhyay, T. Shibata, E.A. Lang, V.N. Zyryanov, B. Ravel, K. McIvor, K.M. Kemner, K.G. Scheckel, S.R. Bare, J. Terry, S.D. Kelly, B.A. Bunker, C.U. Segre, The New MRCAT (Sector 10) Bending Magnet Beamline at the Advanced Photon Source, AIP Conference Proceedings, 1234 (2010) 299-302.

[17] M. Newville, P. Līviņš, Y. Yacoby, J.J. Rehr, E.A. Stern, Near-edge x-ray-absorption fine structure of Pb: A comparison of theory and experiment, Physical Review B, 47 (1993) 14126-14131.

[18] M. Newville, B. Ravel, D. Haskel, J.J. Rehr, E.A. Stern, Y. Yacoby, Analysis of multiple-scattering XAFS data using theoretical standards, Physica B: Condensed Matter, 208–209 (1995) 154-156.

[19] C.O. Dimkpa, D.E. Latta, J.E. McLean, D.W. Britt, M.I. Boyanov, A.J. Anderson, Fate of CuO and ZnO Nano- and Microparticles in the Plant Environment, Environmental Science & Technology, 47 (2013) 4734-4742.

[20] P.A. O'Day, N. Rivera, R. Root, S.A. Carroll, X-ray absorption spectroscopic study of Fe reference compounds for the analysis of natural sediments, American Mineralogist 89 (2004) 572-585.

[21] A. Manceau, M.A. Marcus, N. Tamura, Quantitative Speciation of Heavy Metals in Soils and Sediments by Synchrotron X-ray Techniques, Reviews in Mineralogy and Geochemistry, 49 (2002) 341-428.

[22] S. Ghose, The crystal structure of hydrozincite, $Zn_5(OH)_6(CO_3)_2$, Acta Crystallographica, 17 (1964) 1051-1057.

[23] D.L. Graf, CRYSTALLOGRAPHIC TABLES FOR THE RHOMBOHEDRAL CARBONATES, American Mineralogist, 46 (1961) 1283-1316.

[24] K. Kihara, G. Donnay, Anharmonic thermal vibrations in ZnO, The Canadian Mineralogist, 23 (1985) 647-654.

[25] F. Marumo, Y. Syono, The crystal structure of Zn2SiO4-II, a high-pressure phase of willemite, Acta Crystallographica Section B, 27 (1971) 1868-1870.

[26] J.L. Anderson, R.C. Peterson, I. Swainson, The atomic structure of deuterated boyleite $ZnSO_4{\cdot}4D_2O$, ilesite $MnSO_4{\cdot}4D_2O$, and bianchite $ZnSO_4{\cdot}6D_2O$, American Mineralogist, 97 (2012) 1905-1914.

[27] S.M. Hayes, P.A. O'Day, S.M. Webb, R.M. Maier, J. Chorover, Changes in Zinc Speciation with Mine Tailings Acidification in a Semiarid Weathering Environment, Environmental Science & Technology, 45 (2011) 7166-7172.

[28] H.L. Clever, M.E. Derrick, S.A. Johnson, The Solubility of Some Sparingly Soluble Salts of Zinc and Cadmium in Water and in Aqueous Electrolyte Solutions, Journal of Physical and Chemical Reference Data, 21 (1992) 941-1004.

[29] S.-G. Lee, M.-H. Kim, D.-J. Kim, Y.-J. Lee, Fate and transport of zinc in a sand tank model: monitoring of 2-D plume using TDR method, Environmental Earth Sciences, 72 (2014) 1-9.

[30] S.I. Alghanmi, A.F. Al Sulami, T.A. El-Zayat, B.G. Alhogbi, M. Abdel Salam, Acid leaching of heavy metals from contaminated soil collected from Jeddah, Saudi Arabia: kinetic and thermodynamics studies, International Soil and Water Conservation Research, 3 (2015) 196-208.

[31] I. Ko, C.-H. Lee, K.-P. Lee, S.-W. Lee, K.-W. Kim, Remediation of soil contaminated with arsenic, zinc, and nickel by pilot-scale soil washing, Environmental Progress, 25 (2006) 39-48.

Figure Captions

Figure 1. Study area and sampling locations

Figure 2. Zinc K-edge XANES (left) and EXAFS (right) data from samples MJK-1 to MJK-6-2 compared to the standards that were most similar to the endmember spectra.

Figure 3. Zinc K-edge XANES (left) and EXAFS (right) data from endmember sample MJK-6-2 compared to several O-coordinated Zn(II) standards

Figure 4. Zinc K-edge EXAFS data from endmember sample MJK-6-2 compared to standards. Fourier transform parameters are $\Delta k = 2.2 – 10.5$ Å^{-1} using 1.0 Å^{-1} wide Hanning window sills

Figure 5. Fractions of Zn (%) in contaminated soils. Sequential extraction was employed to evaluate solid-state speciation of Zn in contaminated soils. F1: exchangeable, F2: bound to carbonates, F3: bound to iron and manganese oxides, F4: bound to organic matter, F5: residual

Figure 6. Vertical distribution of toxic metals in contaminated soils. The dashed line indicates the regulatory limit (i.e., the precaution level) of Zn is soil of South Korea

Figure 7. The fractionation of Pb and Zn in soil samples with Tessier sequential extraction procedure. The relation between acid extracted Pb (A) and Zn (B) fraction and F1+F2+F3 fractions of Tessier sequential extraction procedure. The relation between spectral proportions of O-coordinated Zn from LCF and F1+F2+F3 fractions of Tessier sequential extraction procedure (C) and acid extracted Zn fraction (D). The square symbol in (C) indicates the data of Zn-concentrate (MJK-1) which is not included when r^2 is calculated

490

491 Table 1. Chemical and mineralogical properties of samples from study area

Sample		MJK-1	MJK-2	MJK-3	MJK-4	MJK-5-1	MJK-5-2	MJK-5-3	MJK-6-1	MJK-6-2	MJK-6-3
Description		Zn concentrate	Road side dust	Railroad side soil	Railroad side soil	Paddy soil A	Paddy soil A	Paddy soil A	Paddy soil B	Paddy soil B	Paddy soil B
Sampling depth (cm)		-	0	0-15	0-15	0-15	15-30	30-50	0-15	15-30	30-50
Chemical composition[1] (%)	SiO_2	5.72	35.63	46.07	44.17	48.23	47.66	50.14	47.41	49.36	50.23
	Al_2O_3	5.37	12.90	21.73	18.63	21.66	20.93	21.84	17.93	20.52	19.59
	Fe_2O_3	5.73	5.57	8.85	9.20	7.19	6.89	5.35	5.96	7.04	7.55
	K_2O	0.23	2.11	3.87	3.67	4.26	4.22	4.47	4.03	4.70	4.35
	MgO	1.59	2.01	2.07	1.40	1.86	1.79	1.56	2.02	2.22	2.74
	CaO	0.43	18.83	3.06	3.85	1.61	1.64	1.72	6.58	2.60	2.56
	Na_2O	5.88	0.90	0.53	0.40	1.00	1.00	1.39	1.13	0.89	0.99
	TiO_2	0.05	0.45	1.18	0.94	0.91	0.88	0.78	0.78	0.89	1.00
	P_2O_5	0.03	0.24	1.16	0.63	0.42	0.32	0.19	0.34	0.30	0.36
	SO_3	38.66	7.94	0.14	0.99	0.50	0.25	0.08	0.60	0.11	0.08
	ZnO	35.10	11.40	0.21	1.85	0.27	0.17	0.02	0.59	0.13	0.03
	BaO	0.00	0.06	0.11	0.09	0.08	0.11	0.06	0.14	0.13	0.09
	MnO	0.25	0.93	0.87	0.25	0.12	0.11	0.08	0.14	0.17	0.19
	sum	99.04	98.97	89.84	86.06	88.11	85.96	87.68	87.66	89.07	89.76
Soil pH		6.40	8.30	8.70	7.31	7.00	7.80	8.50	8.40	8.40	8.40
LOI (%)		1.8	7.4	6.5	4.4	3.5	1.8	0.6	5.0	3.3	7.7
Toxic metals[2] (mg kg^{-1})	As	2,329.7	198.0	4.2	12.5	61.5	3.3	2.6	6.4	2.4	1.2
	Cd	1,311.4	470.0	7.4	58.8	15.4	4.6	1.5	17.8	4.8	2.1
	Cu	6,689.6	1,121.0	36.2	290.3	36.1	20.7	10.9	58.7	55.1	28.8
	Ni	9.0	< 0.4	22.2	28.7	23.3	15.3	12.6	15.3	18.9	19.7
	Pb	5,138.5	2,312.0	50.6	420.1	87.1	42.4	13.0	140.4	38.3	16.2
	Zn	560,619.0	92,826.0	1,159.9	12,791.0	1,698.70	923.4	100.9	3,551.4	721.9	161.8
Fraction of Zn conc. by sequential extraction[3] (%)	F1	0.1	0.5	0.3	1.4	1.2	0.1	0.4	0.0	0.0	0.1
	F2	0.6	2.6	13.5	7.2	8.4	10.1	2.9	4.9	10.9	5.1
	F3	11.5	4.1	33.1	16.7	35.7	44.0	23.5	16.0	46.6	24.8
	F4	27.7	43.6	35.1	51.0	42.4	30.7	24.7	57.3	23.3	30.2
	F5	60.0	49.1	18.1	23.7	12.4	15.1	48.5	21.7	19.1	39.9
	sum	100.0	100.0	100.0	100.0	100.0	100.0	100.0	100.0	100.0	100.0
Soil color		10YR4/1	10YR6/1	10YR5/4	10YR4/1	10YR6/2	10YR5/2	10YR5/2	10YR6/2	10YR5/4	10YR5/4
Major minerals[4]		Zinc iron sulfide	Silicon oxide	Silicon oxide	Silicon oxide	Quartz	Calcium carbonates	ND*	Silicon oxide	Sodium aluminum sulfate hydrate	ND
			Sphalerite (Fe-rich)	Anorthite		Anorthite, sodian	Silicon oxide		Iron oxide (Fe_3O_4)	Lithium potassium iron aluminum fluoride silicate hydroxide	
			Calcite			Orthopyroxene	Calcite			Silicon oxide	

1) = measured by X-ray Flurorescence(XRF); mean of triplicates
2) = determined by ICP-OES after *aqua regia* digestion
3) = measured by Tessier methods; mean of duplicates; F1=exchangeable, F2=bound to carbonates, F3=bound to iron and manganese oxides, F4=bound to organic matter and sulfides, F5= residual
4) = measured by X-ray powder Diffractometer (pXRD)

* ND = Not Determined

492

493

Table 2. Summary of the best fit component fractions resulting from the LCF (Linear Combination Fit) analysis of the EXAFS data

Sample	Spectral proportions from LCF	
	MJK-1	**MJK-6-2**
MJK-1	100%	0%
MJK-2	89%	11%
MJK-3	11%	89%
MJK-4	40%	60%
MJK-5-1	15%	85%
MJK-5-2	5%	95%
MJK-6-1	53%	47%
MJK-6-2	0%	100%

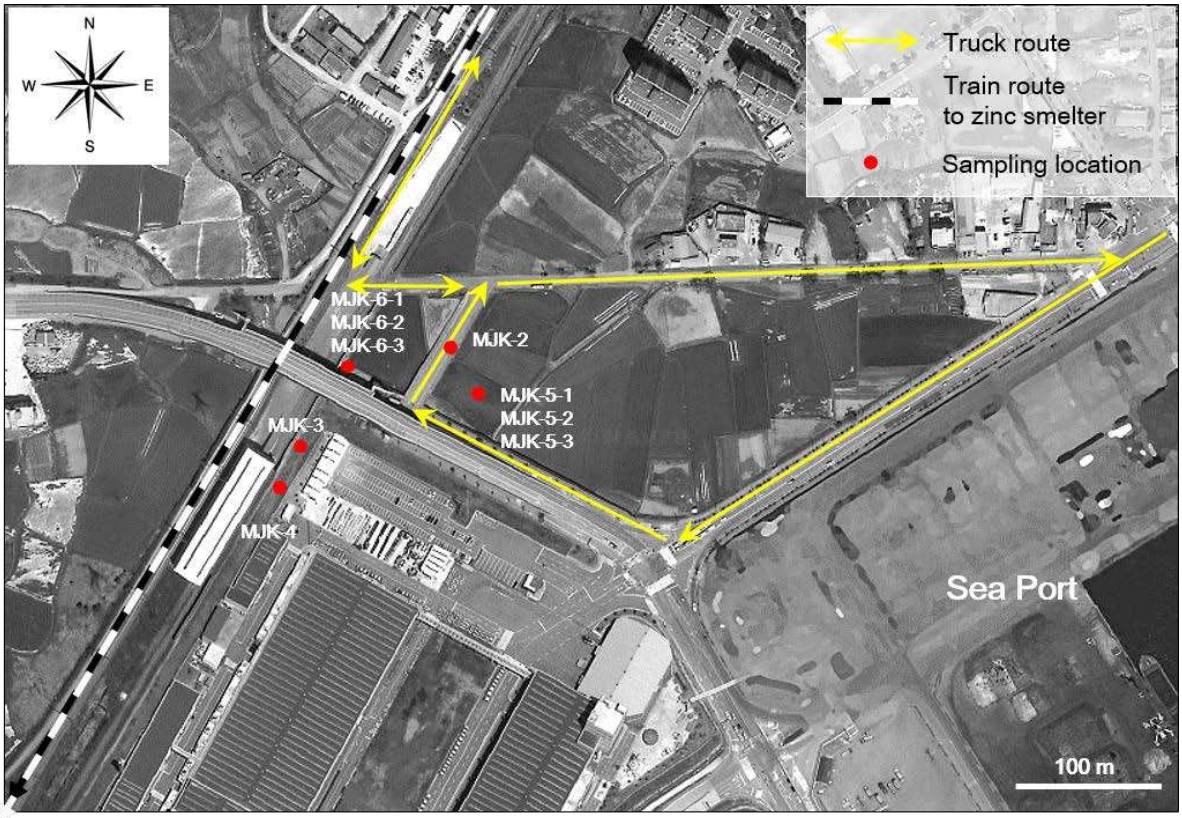
N
W
E
S
Truck route
Train route
to zinc smelter
Sampling location
MJK-6-1
MJK-6-2
MJK-6-3
MJK-2
MJK-5-1
MJK-5-2
MJK-5-3
MJK-3
MJK-4
Sea Port
100 m

Figure 1.

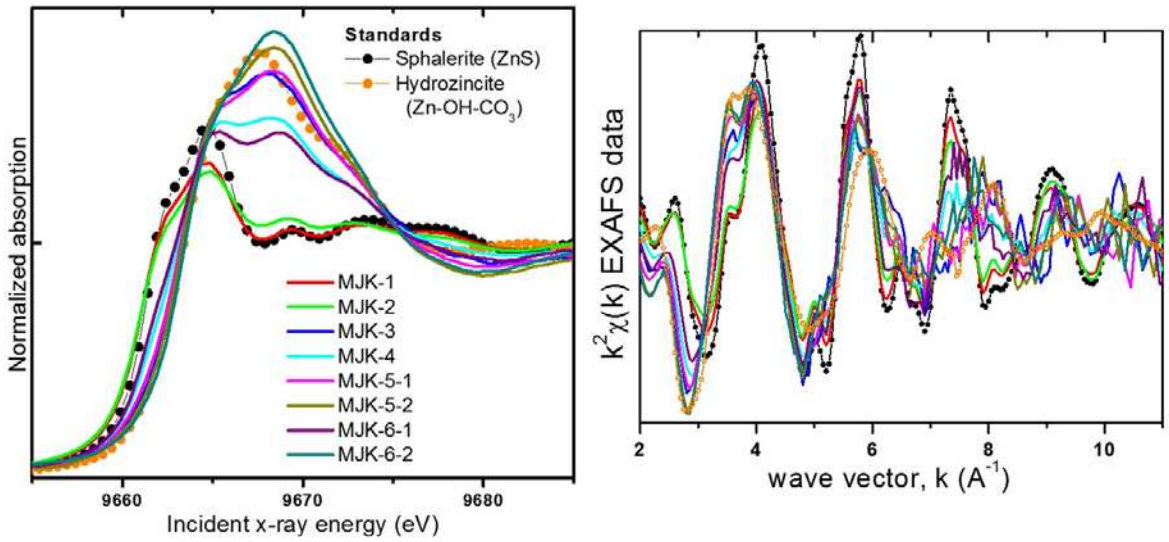
Standards
Sphalerite (ZnS)
Hydrozincite
(Zn-OH-CO3)
MJK-1
MJK-2
MJK-3
MJK-4
MJK-5-1
MJK-5-2
MJK-6-1
MJK-6-2
Normalized absorption
9660
9670
9680
Incident x-ray energy (eV)
k2χ(k) EXAFS data
2
4
6
8
10
wave vector, k (A-1)

Figure 2.

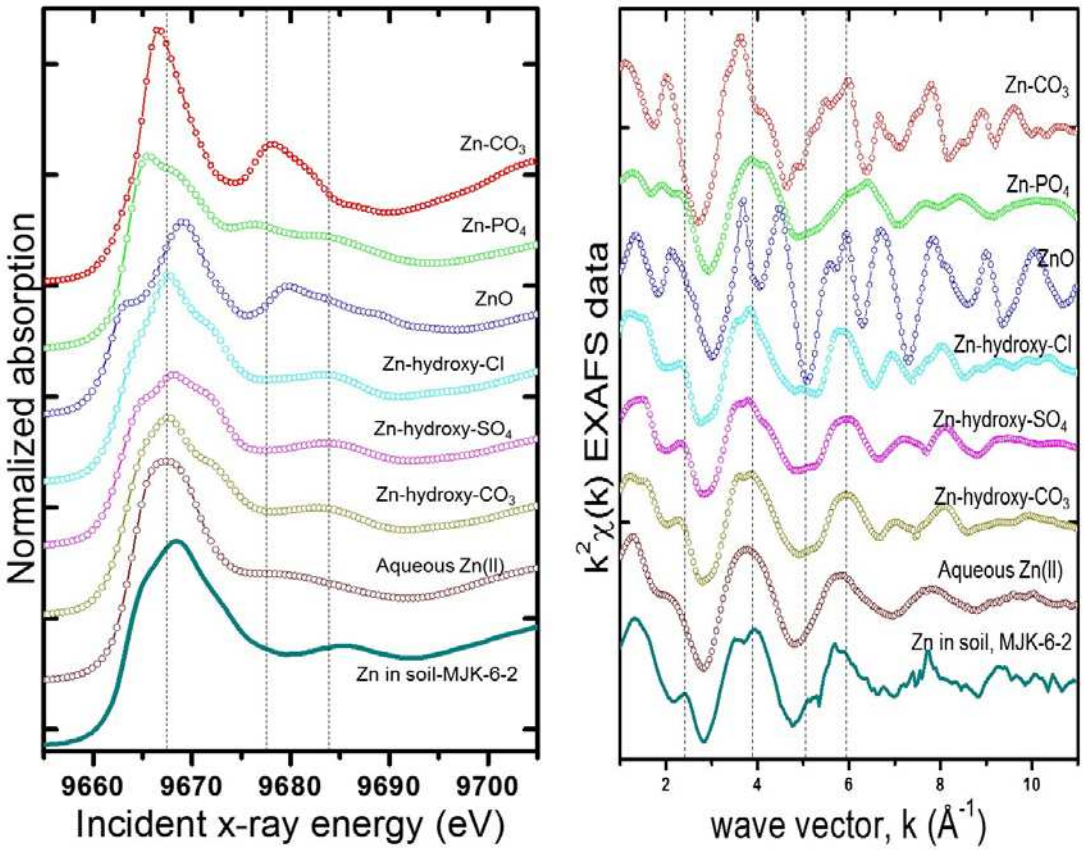

538

539

540 Figure 3.

541

542

543

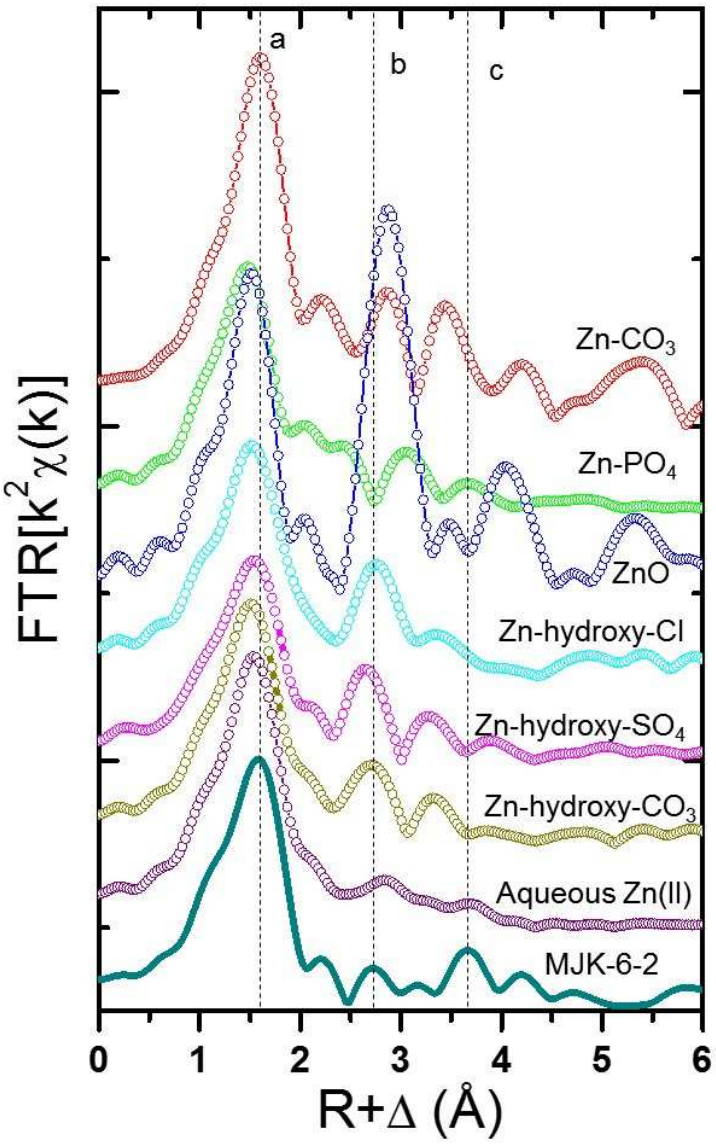

544

545 Figure 4.

546

547

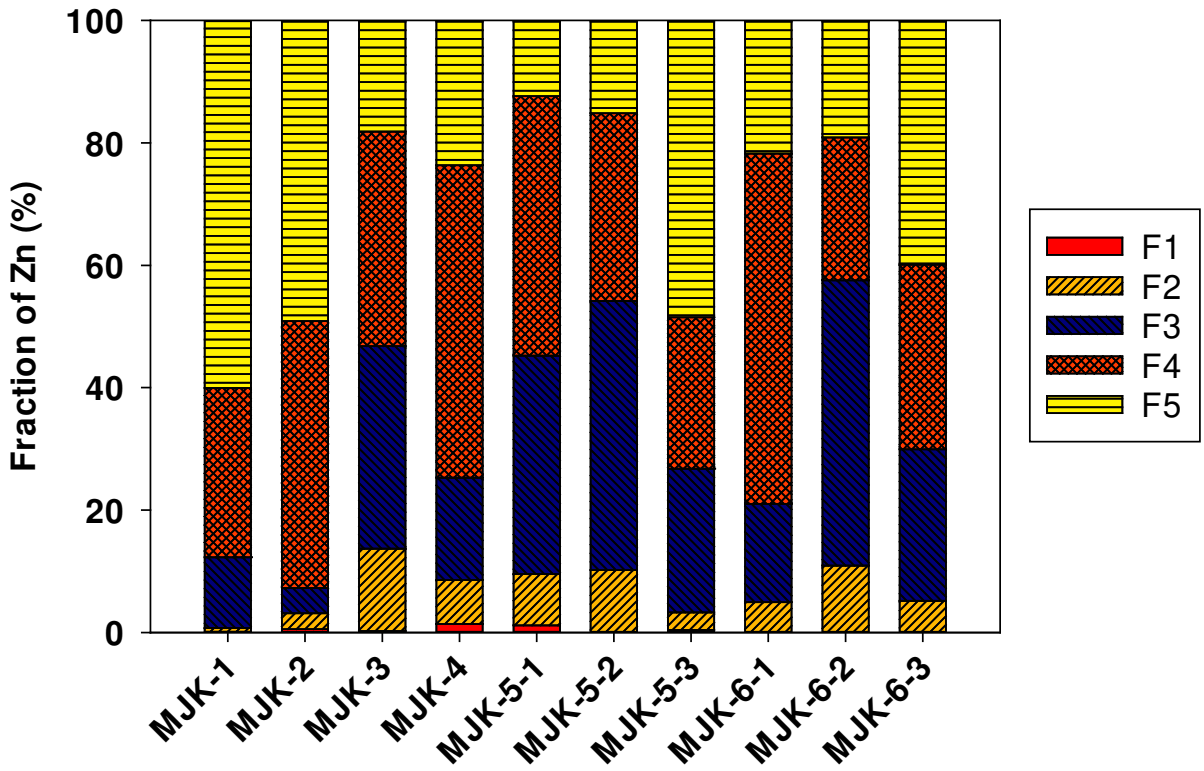

548

549

550 Figure 5.

551

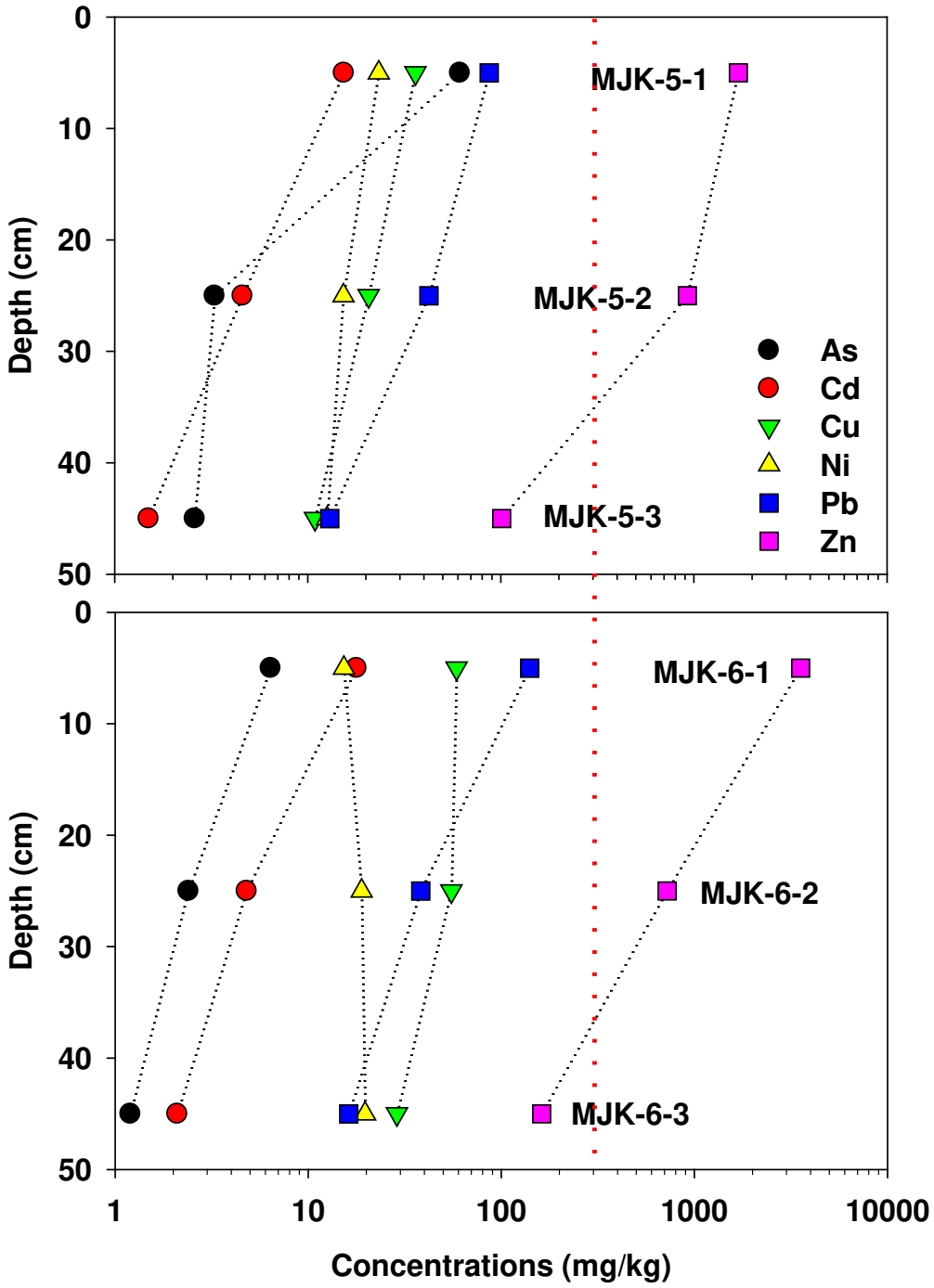

552

553

554 Figure 6.

555

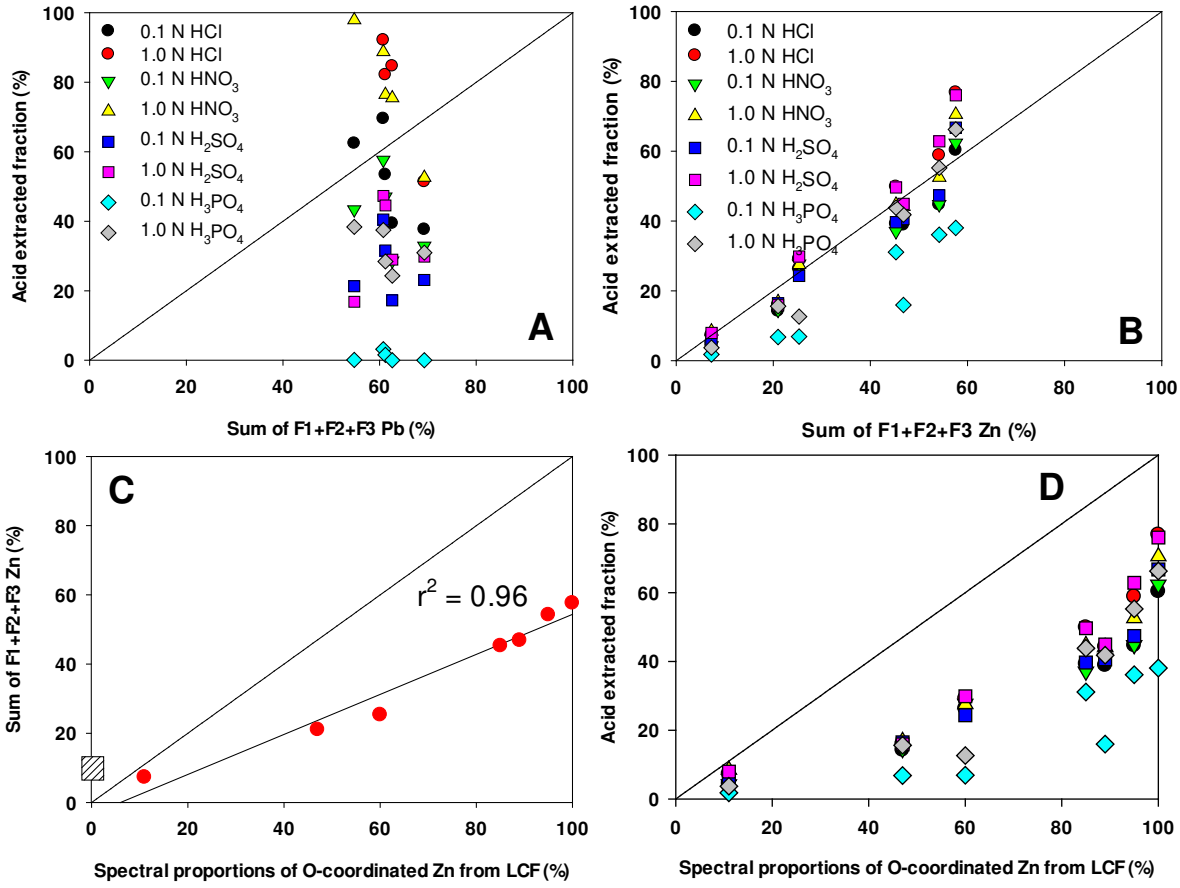

556

557

558

559 Figure 7.

560

561